Acta Materialia 99 (2015) 281–289

Contents lists available at ScienceDirect

Acta Materialia

journal homepage: www.elsevier.com/locate/actamat

Structural transformations among austenite, ferrite and cementite in Fe–C alloys: A unified theory based on *ab initio* simulations

Xie Zhang [a,*], Tilmann Hickel [a], Jutta Rogal [b], Sebastian Fähler [c,d], Ralf Drautz [b], Jörg Neugebauer [a]

[a] Max-Planck-Institut für Eisenforschung GmbH, 40237 Düsseldorf, Germany
[b] Interdisciplinary Centre for Advanced Materials Simulation, Ruhr-Universität Bochum, 44780 Bochum, Germany
[c] IFW Dresden, P.O. Box: 270116, 01171 Dresden, Germany
[d] Institute for Solid State Physics, Department of Physics, Dresden University of Technology, 01062 Dresden, Germany

ARTICLE INFO

Article history:
Received 28 April 2015
Revised 24 July 2015
Accepted 30 July 2015

Keywords:
Structural phase transition
Fe–C alloys
Ab initio simulations

ABSTRACT

Structural transformations in Fe–C alloys are decisive for the mechanical properties of steels, but their modeling remains a challenge due to the simultaneous changes in Fe lattice and redistribution of C. With a combination of the orientation relationships between austenite, ferrite and cementite, we identify a metastable intermediate structure (MIS), which can serve as a link between the three phases. Based on this framework, different mechanisms depending on the local conditions (C concentration, strain, magnetism) are revealed from *ab initio* nudged elastic band simulations, which allow us to construct a unified theory for the structural transformations among austenite, ferrite and cementite.

1. Introduction

The kinetics of structural phase transitions belongs to the most fundamental and fascinating fields of materials science and condensed matter physics [1–4]. One of the materials that owes many of its extraordinary mechanical properties to structural phase transitions is the Fe–C system, the basis of steels. While one would assume that Fe–C belongs to the best studied materials (see e.g., [5–8]), the atomistic processes involved in the structural transformation from the high-temperature face-centered cubic (fcc) austenite to the low-temperature body-centered cubic (bcc) ferrite are still insufficiently understood. This does not only apply to the complicated thermodynamics of the cooling process, but also to structural relationships independent of temperature [9].

The complexity of the transformation is mainly due to the combination of the two subsystems, Fe and C. Considering on the one hand the Fe atoms only, the martensitic rearrangement of the atoms from fcc to bcc is typically described by processes like the Bain path. This assumes a homogeneous transition of the whole grain and cannot account for large lattice mismatches that occur when considering the more realistic scenario of a moving austenite/ferrite interface during cooling. An atomistic investigation of possible adaptation processes [10] at the interface has so far not been performed for steels. The C atoms, on the other hand, occupy interstitial positions in Fe lattices, but show a remarkably lower solubility in bcc Fe as compared to fcc Fe. Therefore, a redistribution of C atoms is required when the austenite/ferrite interface moves during cooling. Thermodynamically, this is captured by the formation of orthorhombic cementite (Fe_3C) precipitates during cooling. However, this requires local C concentrations in the order of 25 at.%, which cannot be the result of random fluctuations, but only a well-defined nucleation process. Again, an atomistic understanding of this nucleation process is currently missing.

We believe that only a sophisticated atomic-scale interplay between the change of the Fe matrix and the redistribution of C can explain the complex transformations of the Fe–C system among austenite, ferrite and cementite. We therefore employ first-principles calculations to obtain atomistic insights into underlying mechanisms as well as details about the crystallographic orientation relationships (ORs) and the energetics of the different phases. Our study reveals the occurrence of a metastable intermediate structure (MIS), which acts as a central connection among austenite, ferrite and cementite. Depending on the local conditions (C concentration, strain, magnetism) different mechanisms are observed for the transformations between the MIS and the three phases. However, the MIS is not a stable bulk phase, but acts as a buffer layer at the austenite/ferrite and austenite/cementite interfaces similar to the concept of complexions [11]. The formation of the MIS is triggered by interface reconstructions and it can further facilitate the decomposition of austenite into ferrite and cementite. With these insights a clear atomistic picture how the phase

* Corresponding author.
E-mail address: x.zhang@mpie.de (X. Zhang).

http://dx.doi.org/10.1016/j.actamat.2015.07.075
1359-6454/

transformations among austenite, ferrite and cementite can happen at the interfaces is thus provided.

In the following, we will firstly describe our computational details in Section 2. Secondly, the lattice correspondence between austenite, ferrite and cementite is established and illustrated in Section 3. Then we evaluate the minimum energy paths (MEPs) of the structural transformations in bulk under different conditions and discuss the corresponding mechanisms of the atomistic processes in Section 4. Moreover, we combine all the phases/structures at the interfaces and try to interpret a realistic picture for the phase transformations among austenite, ferrite and cementite in Section 5. In addition, all the aspects that need to be considered to prove this picture are also discussed in this section. Finally, the achievement of this work is summarized in Section 6.

2. Computational details

All *ab initio* calculations in this work are performed employing spin-polarized density functional theory (DFT). For the description of the electron–ion interactions, we use Blöchl's projector augmented wave (PAW) potentials [12] combined with the Perdew–Burke–Ernzerhof (PBE) parameterization [13] of the exchange–correlation functional, as implemented in the Vienna *Ab Initio* Simulation Package (VASP) [14].

In order to produce reliable calculation results, systematic convergence tests are carried out for fcc and bcc Fe as well as the orthorhombic Fe_3C unit cells. It is found that the use of a plane-wave energy cutoff E_{cut} = 400 eV, and ~10,000 **k**-points × atoms resulting from a homogeneous Monkhorst–Pack sampling [15] of the Brillouin zone can ensure accurate descriptions of the three phases (the lattice constants converge to a computational error of less than 0.001 Å and the maximum deviation from experimental results is 0.94%). A first order Methfessel–Paxton scheme [16] with a thermal smearing parameter of 0.2 eV is used for integration over the **k**-points. The optimized lattice constant and local magnetic moment of the ferromagnetic high-spin (FM-HS) fcc Fe are 3.640 Å and 2.5 μ_B/atom, respectively. Those of the FM bcc Fe are 2.834 Å and 2.2 μ_B/atom, respectively. The lattice constants of cementite are also optimized and provided in Table 1. The local magnetic moments of Fe atoms in cementite in the two sublattices are 1.97 μ_B/atom (Fe_{4c}) and 1.88 μ_B/atom (Fe_{8d}), respectively. Both the optimized structural and magnetic properties of the three phases show good agreement with previous experimental data and theoretical results [17–19,8].

For the paramagnetic (PM) calculations of austenite and the MIS, we employ the special quasi-random structures (SQS) approach as implemented in the ATAT code [20]. The SQS is originated from the cluster expansion method which is based on the generalized Ising model. Spin-up (50%) and spin-down (50%) moments (±2.4 μ_B/atom) are randomly distributed within a 1.5 × 1 × 2 supercell (36 Fe atoms) using a binary SQS. Notably, here we have a multiple of 1.5 because the unit cells for austenite, ferrite and the MIS as will be shown in Fig. 1 are not primitive.

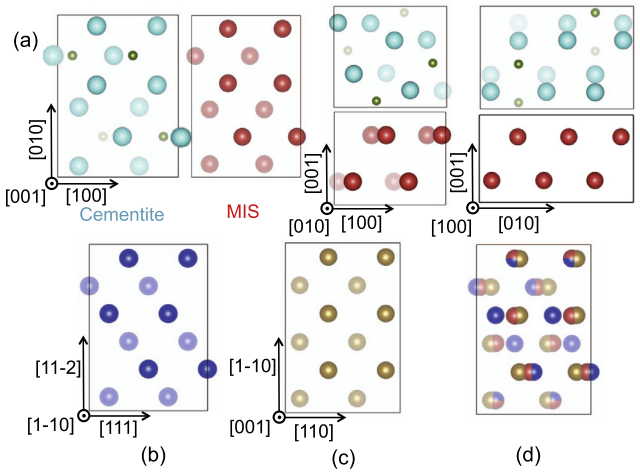

Fig. 1. (a) shows the comparison between cementite and the MIS in three projections. Large spheres represent Fe atoms and small green spheres refer to C. In the second row the orthorhombic unit cells of ferrite (b) and austenite (c) are shown. In (d) a comparison of the atomic positions of the MIS, ferrite and austenite is shown. Lower-lying atoms are shaded with gray color. The structures in this paper are visualized with the VESTA program [36]. (For interpretation of the references to color in this figure caption, the reader is referred to the web version of this article.)

Table 1
Optimized lattice constants of the orthorhombic cells of austenite, ferrite, the MIS and cementite. All values are given in Å.

Phases/structures	*a*	*b*	*c*
Austenite (before tetragonal distortion)	5.148	7.722	3.640
Austenite (after tetragonal distortion)	4.841	7.264	4.016
Ferrite	4.909	6.942	4.008
MIS (without C)	4.860	7.164	4.033
MIS (25 at.% C)	5.415	7.670	3.919
Cementite	5.038	6.727	4.484

3. Lattice correspondence between austenite, ferrite and cementite

To unify the phase transitions among austenite, ferrite and cementite, a consistent description of the lattice correspondence is required. This motivates us to seek for a combination of the commonly observed ORs between austenite, ferrite and cementite [21–35]. In reality, the transformation behavior of Fe and C redistribution are always coupled, in particular if cementite is involved. However, in our aim to disentangle the two aspects [namely, the change in Fe lattice and the C redistribution] we artificially remove for a moment all C atoms from the crystal structure of cementite (Fig. 1) and fully relax it (volume, cell shape and atomic positions) using DFT calculations. The optimized structure is for reasons that become clearer below labeled as "MIS" (short for metastable intermediate structure) in Fig. 1(a) and the lattice constants are given in Table 1. Comparing this optimized structure to cementite it can be seen that the overall arrangement of Fe atoms is very similar for the projection in the (001) plane, but significant atomic shifts are observed for the other two projections.

To understand how the MIS relates to austenite and ferrite, we investigate different ORs. For ferrite an orthorhombic cell can be constructed (shown in Fig. 1(b)) with which the correspondence of the atomic positions to those in the MIS becomes clearly visible. This orthorhombic cell of ferrite captures the general idea behind the Bagaryatsky OR [27,35]. For austenite the previously reported ORs between austenite and cementite [31–34] do not provide a suitable unit cell. To achieve a lattice correspondence between austenite and the MIS we construct the orthorhombic unit cell shown in Fig. 1(c). This orientation has to our knowledge not been used before to describe the OR between austenite and cementite, but a similar concept has been used by Pitsch [25] to discuss the OR between austenite and martensite. Comparing the atomic positions of the MIS and the chosen representation of ferrite and austenite as shown in Fig. 1(d), one can already now realize that the MIS does crystallographically act as an intermediate step for the austenite → ferrite transition. This role will be further validated by our simulations below.

4. Structural transformations

In reality, the transformation of austenite into ferrite and cementite does not involve the entire austenitic phase, but only a small part at the moving interface. However, it is technically unfeasible to simulate such a scenario with DFT. Hence, in this work we mimic the situation at the interface by investigating the structural transformations among the four bulk structures under different *local conditions* and determine the role of the MIS in this context. However, as will be shown in Section 5, the MIS is not an isolated bulk phase, but an interface structure. The investigations in this section illustrate how the MIS is structurally linked to austenite, ferrite and cementite, and which local conditions might trigger the transformations between the MIS and the three phases. To calculate the MEPs along the transformation we use the solid-state nudged elastic band (SSNEB) method [37] with energetics based on DFT as implemented in the VTST code [38,39]. In this way the transformation on the $T = 0$ K potential energy surface is characterized. For the three different transitions we identify three different mechanisms that are triggered by the respective *local conditions*, including C concentration, strain and magnetism. In this section, we discuss the three transitions separately and we will combine our findings to interpret a unified picture in the next section.

4.1. Austenite → MIS transition

Regarding the austenite → MIS transition, the magnetic state of austenite is important. The high temperature austenitic phase is known to be stable in the PM state. However, the transformation temperature for the case of cementite formation, is below 1000 K [40], which is lower than the Curie temperature of bcc Fe, 1044 K [41]. Taking into account additional undercooling, the product ferritic phase is FM instead of PM. This indicates that both structural and magnetic phase transitions simultaneously happen at the austenite/ferrite interface, which makes the magnetic state of the MIS complex and not well defined. Due to the technical difficulty of electronic convergences of these magnetic degrees of freedom in common DFT codes, it is unfeasible to calculate the MEP for a transition of PM austenite → FM ferrite. Therefore, for the austenite → MIS transition we consider two limiting cases: (a) FM austenite → FM MIS and (b) PM austenite → PM MIS.

Within the FM-HS state, fcc Fe is unstable and can directly relax to a face-centered tetragonal (fct) state with $c/a = 1.17$. Hence, the initial geometry of austenite is treated as fct in the FM-HS state. The MEP of the austenite (FM, fct Fe) → MIS (without C) transition is shown in Fig. 2(a). It can be seen that this is actually a barrier-free transition. Vice versa, if we perform PM calculations for the MIS, it would be dynamically unstable and easily relaxes to PM fcc austenite. Since it is a direct relaxation and not really a MEP, it is therefore not shown in Fig. 2(a).

In addition, if one considers the antiferromagnetic single-layer (AFMS), antiferromagnetic double-layer (AFMD) or ferromagnetic low-spin (FM-LS) states, the MIS is also dynamically unstable and relaxes to fcc/fct Fe directly. This demonstrates the close relation between the MIS and austenite, and implies that a transition from austenite to the MIS could be triggered by a local FM ordering at the interface, though the specific barrier for the magnetic transition is not directly accessible (details will be given in the next section).

4.2. MIS → ferrite transition

In order to further decompose the MIS into ferrite and cementite, C redistribution is required. To investigate if there is a thermodynamic driving force for the decomposition we calculate the stability of austenite, the MIS, ferrite and cementite as a function of C concentration. As shown in Fig. 3 for a single phase, ferrite is most stable for C concentrations lower than ~19 at.%, while cementite is the stable phase for higher C concentrations (>19 at.%). We can further observe that for the shown range of C concentration it would always be thermodynamically favorable for the system to decompose into ferrite (with 0 at.% C) and cementite (with 25 at.% C), as shown by the orange line in Fig. 3. Hence, there exists a clear thermodynamic driving force for the MIS (with several at.% C from austenite) to decompose.

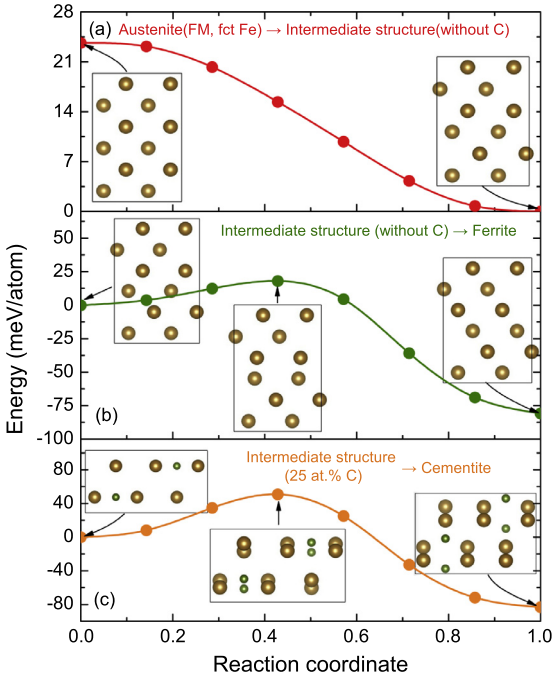

Fig. 2. Minimum energy paths for (a) austenite (FM, fct Fe) → MIS (without C), (b) MIS (without C) → ferrite, and (c) MIS (25 at.% C) → cementite transformations. Large spheres indicate Fe atoms in different phases/structures, while small spheres indicate C atoms.

The MEP of the transition of the MIS without C → ferrite is shown in Fig. 2(b). It can be seen that an energy barrier of only ~18 meV/atom needs to be overcome. The mechanism of this transformation is mainly dominated by a shear like shuffle along $[1\,1\,1]_{\text{ferrite}}$ of the two central atomic layers. This implies that the MIS can actually be viewed as the result of arranging planar defects in bcc Fe along the $[1\,1\,\bar{2}]_{\text{bcc}}$ direction periodically. To be more specific, as shown in Fig. 4, such a planar defect corresponds to the formation of two Σ3 twin boundaries in bcc Fe. It has been shown [43] that there exists a clear driving force for C to segregate to Σ3 grain boundaries in bcc Fe. Hence, the structural feature of the MIS makes it a perfect place for C to accumulate. The C redistribution becomes thus feasible and physically understandable. Details of the kinetics of such segregation processes require further investigations, but are beyond the scope of this paper. Once the accumulated C content in the MIS reaches the order of 25 at.% (or at least ⩾19 at.%), the formation of cementite becomes possible and will be clarified in the next subsection.

4.3. MIS → cementite transition

Having a local accumulation of C in the MIS we investigate the second part of the decomposition, the transition of the MIS with 25 at.% C → cementite. The MEP of the transition in Fig. 2(c) shows an energy barrier of ~51 meV/atom. Since the size of nucleus is

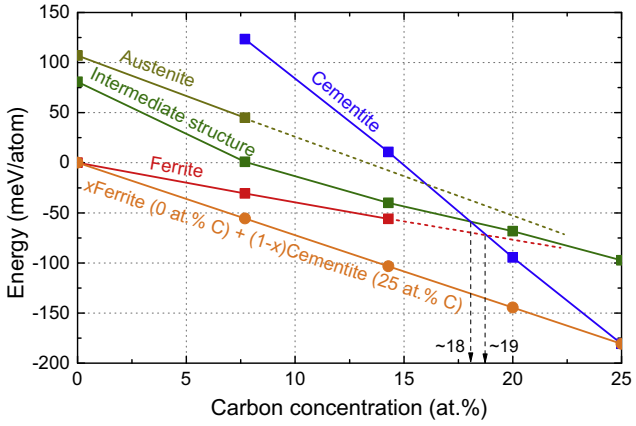

Fig. 3. Stability of austenite, ferrite, cementite and the MIS with respect to C content. The energies of cementite and the MIS with respect to C content are calculated by introducing different numbers of C atoms at the interstitial sites in one unit cell. The curve of ferrite is calculated with two different strategies. The very left two dots are calculated with pure bcc Fe and placing one C at an octahedral site, respectively. For the third dot, all the possible configurations (630 configurations in total) for placing two C atoms at any two of all the 36 octahedral interstitial sites in the orthorhombic cell of ferrite are firstly evaluated by an Fe–C EAM potential [42] including full relaxation. The five lowest energy configurations are then fully relaxed using DFT and the calculated energy difference between the five configurations is found to be less than 0.1 meV/atom. For higher C concentrations we assume a linear dependence of the energy on the C content. Similar calculations are performed for FM austenite. However, we only obtain the very left two dots because for higher C contents, it directly relaxes to the MIS. The energies are defined as $E = E_{tot}/N_{Fe+C} - E$(bcc Fe without C), where E_{tot} is the total energy of the cells including different number of C atoms. N_{Fe+C} is the total number of Fe and C atoms in the cell. We do not use the formation energy because the formation energy would require the reference chemical potential for C, which creates additional problems (graphite vs. diamond). Graphite is more realistic, but cannot be appropriately described by conventional exchange–correlation functionals in DFT due to the van der Waals interaction.

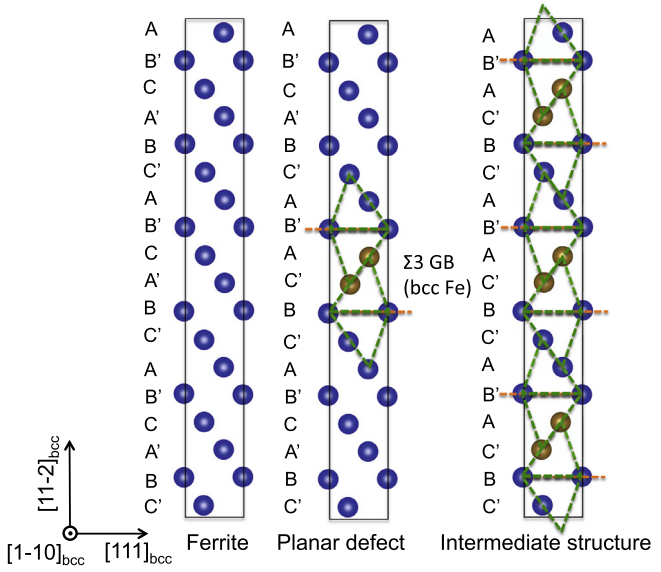

Fig. 4. Interpretation of the MIS as the result of a periodic stacking of the Σ3 grain boundary in bcc Fe. On the left side of each structure, the stacking sequence is provided. The stacking periodicity in bcc lattice is 6 atomic layers, i.e., AB′CA′BC′ as a period. The label letters with/without "prime" correspond to the front/back layer in [1$\bar{1}$0] direction.

unclear and temperature effects are not taken into account, the absolute value of the energy barrier does not make much sense. However, a fair comparison to the energy barrier of the

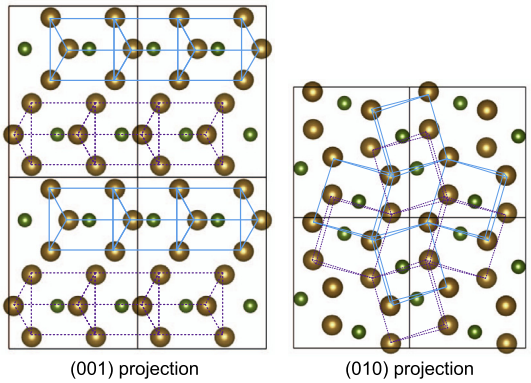

Fig. 5. Interpretation of the crystal structure of cementite. Large gold spheres represent Fe atoms and small green spheres refer to C.

MIS → ferrite transition indicates that the MIS → cementite transition is the rate-limiting process.

To better understand the transformation mechanism, we revisit the crystal structure of cementite. Fig. 5 shows a detailed interpretation of the crystal structure of cementite. Based on the projection of a $2 \times 2 \times 2$ supercell of cementite in the (001) plane, one can clearly identify that cementite has a two-layered structure (marked by two different colors: light blue (solid) and purple (dashed)). For each layer, there exists a consistent and also well defined building block, namely, the trigonal prism. Each trigonal prism consists of six Fe atoms (corners) and one C atom (center). From the projection in the (010) plane, it can be easily seen that each layer of cementite is formed by a zig-zag stacking of the trigonal prisms. The major difference between the two layers is the orientation of the trigonal prisms.

During the MIS → cementite transition (Fig. 6), the C atoms are initially sitting at the octahedral sites (the face centers of the prisms) and then move to the center of the prisms. We find that the energy barrier along the transition path results from the migration of C from the face to the center of the trigonal prisms and the Fe matrix then barrierlessly rearranges itself in a zig-zag way, accordingly.

5. Phase transformation mechanisms at interfaces

Combining all the above results and discussion on the structural transformations among austenite, ferrite and cementite, we are now able to suggest a unified picture for the realistic phase transformations among the three phases. In this section, we will first discuss the atomistic picture how the phase transformations could happen in reality in Section 5.1. Then we will discuss all the aspects that need to be taken into account to fully prove this picture in Sections 5.2–5.4.

5.1. Phase transformation mechanisms

A schematic representation of the austenite/ferrite/cementite interfaces is constructed with the identified ORs between the four structures in Fig. 7. The MIS acts as a central link between all three phases at the interface, which makes the decomposition of austenite into ferrite and cementite physically intuitive and structurally possible. To understand the phase transformation mechanisms, the key is then to understand the features of the MIS and how it evolves under different conditions. Specifically, the presence of the MIS has two important consequences in this system:

First, the MIS acts like a buffer zone between the different phases during the decomposition similar to the concept of

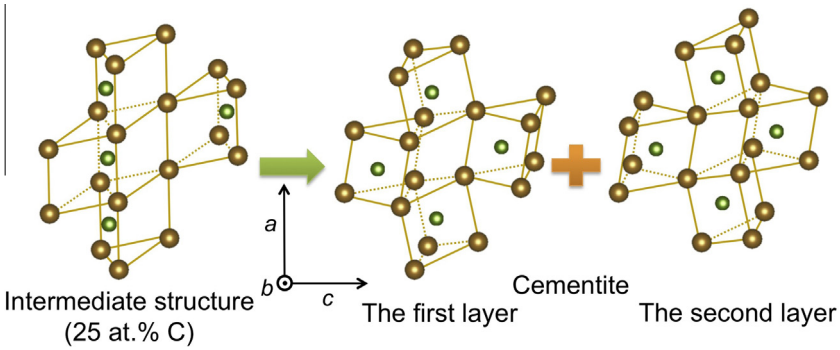

Fig. 6. Schematic of the formation of cementite from the MIS by C migration from the octahedral site to the center of the trigonal prisms. Large spheres represent Fe, while small spheres represent C.

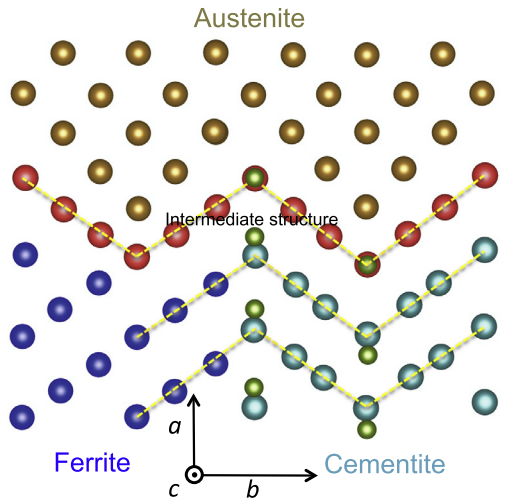

Fig. 7. Representation of the atomistic mechanism of austenite decomposition including the effect of interfaces. Large spheres refer to Fe atoms in austenite (gold), the MIS (red), ferrite (blue) and cementite (cyan). Small green spheres refer to C atoms. Yellow dashed lines visualize the formed nano-twins during decomposition. The three directions a, b and c are defined as the [100], [010] and [001] directions in the unit cell of cementite as shown in Fig. 1. (For interpretation of the references to color in this figure caption, the reader is referred to the web version of this article.)

complexions [11]. As will be shown in the following subsections, it is not a stable bulk phase, but only survives within 2–3 atomic layers at the interface. It is formed naturally by interface reconstructions in order to minimize the interface energy. In the previous discussion we have already mentioned several reasons, why the direct interface between perfect austenite and ferrite is very unfavorable: (a) they have different magnetic orderings; (b) the lattice mismatch between them is quite pronounced (in the order of 10%); (c) they have different atomic arrangements and cannot nicely match each other at the interface. Once an interface reconstruction is involved, the ferromagnetism in ferrite penetrates into austenite by 2–3 atomic layers and thus induces a local FM ordering in austenite (see the discussion in Section 5.3). Since the FM austenite is dynamically unstable, it transforms easily to the FM MIS by minor atomic displacements. Also, during the interface reconstruction, the MIS retains structural similarities to both austenite and ferrite involved in the interface, which makes the transitions to different phases structurally very clear. How it evolves during the phase transition, is mainly dominated by the local conditions. It will transform to austenite if the local magnetic state becomes PM. Within the FM state, it can either transform to ferrite or cementite depending on the local C concentration: If the local C concentration is close to zero, it transforms to ferrite while if the local C content is larger than 19 at.%, it turns to cementite. Since it is always energetically less stable against phase separation into ferrite and cementite in bulk, it will continuously perform this decomposition. However, it will also be constantly formed otherwise the austenite/ferrite and austenite/cementite interfaces would be unfavorable. Thus the phase transformation proceeds along with a moving interface.

Second, it can be considered as a modulated structure of austenite that results in a periodic arrangement of Σ3 nano-twin boundaries of bcc Fe. Due to such a twin feature, it provides the structural environment to accumulate C, which is a precursor for forming cementite. Since it contains a large number of periodic Σ3 twin boundaries, it can ensure that a newly formed interface between ferrite and cementite during the decomposition has the character of a twin boundary and is thus energetically favorable. This applies to a varied ratio between ferrite and cementite resulting from different initial C content in austenite.

The interpretation of the MIS as a twin is analogous to the concept of adaptive phase formation proposed by Khachaturyan et al. [10] to explain the appearance of an intermediate phase during the martensitic transition. In their picture, the intermediate martensite can be regarded as an adaptive twin, which forms as an elastically constrained phase to accommodate the large lattice mismatch between austenite and martensite. This idea has recently been experimentally validated in the Fe–Pd system [44]. Similarly, in Fe–C alloys, the MIS forms by tetragonal deformation and twinning in order to stabilize the FM ordering and accommodate lattice mismatches at the austenite/ferrite interface.

Hence, the relevance of the MIS as a buffer zone as well as a microstructure for C accumulation, is intrinsically related to the physical nature of the interface. In the following we will provide further support for this picture by discussing three special aspects. Due to methodological limitations, this cannot have the character of a rigorous proof, but reflects the best achievable insights one can currently obtain from DFT calculations.

5.2. Interface energies

To demonstrate the decisive role of interfaces in the phase transitions, the interface energies are of interests and importance. Hence, we systematically investigate them for the interfaces involved. For the binary interfaces between ferrite and cementite (or the MIS), the supercell is constructed by combining the unit cells of ferrite and cementite (or the MIS) shown in Fig. 1 using the (0 1 0) plane as the habit plane. Lattice parameters at the interfaces are optimized in both directions within the habit plane. Specifically, the interface between ferrite and cementite is stable and its energy is calculated with a structural setup (Bagaryatsky OR) shown in Fig. 8(e) as 28.3 meV/Å^2 (0.45 J/m^2), which is

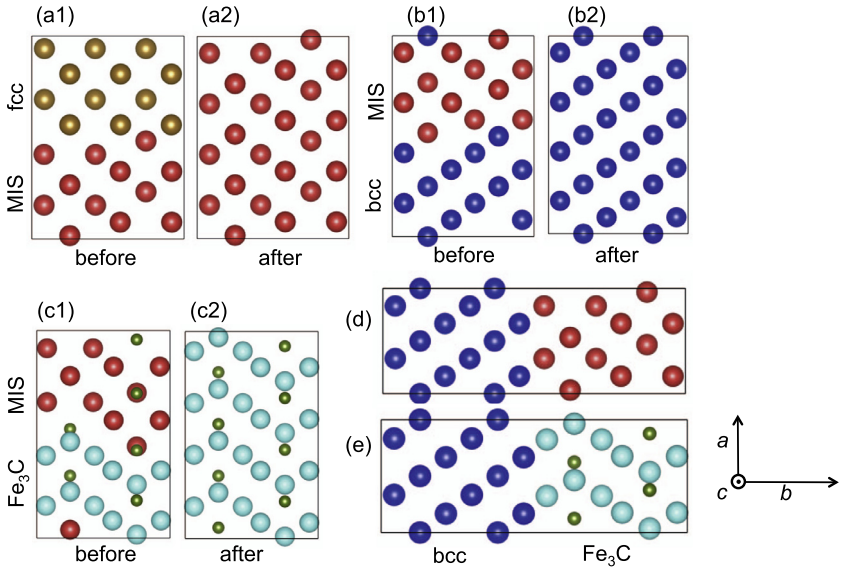

Fig. 8. Atomic structures of the interfaces. (a1) shows the supercell setup for the interface between austenite and the MIS. (a2) presents the result of (a1) after relaxation. Similarly, the supercells for the interfaces between the MIS and ferrite, the MIS and cementite before and after relaxation are given in (b1) and (b2), (c1) and (c2), respectively. (d) and (e) represent the interfaces between ferrite and cementite without and with C, respectively. The directions a, b and c are defined the same as those in Fig. 7. Note that to reduce the space we only show a very small supercell, yet we did check the cell size convergence and performed calculations with much larger supercells.

comparable with the energy of the Σ3 grain boundary in bcc Fe (0.47 J/m^2 [45]). If we further neglect C, then cementite relaxes to the MIS. Thus we can also construct a purely twinned interface between ferrite and the MIS as shown in Fig. 8(d), the interface energy is only 1.7 meV/Å^2 (0.027 J/m^2), which is even smaller. This supports that the newly formed interface between ferrite and cementite is energetically favorable.

In addition, we look at the three possible binary interfaces between the MIS and the three bulk phases: austenite (Fig. 8(a1)), ferrite (Fig. 8(b1)), and cementite (Fig. 8(c1)). However, as shown by Fig. 8(a2), (b2) and (c2), the three interfaces are all unstable against atomic relaxations within the FM state, though there are actually barriers for the MIS → ferrite and the MIS (25 at.% C) → cementite *bulk* transitions. Notably, the binary interface between ferrite and the MIS shown in Fig. 8(b1) is different from the one shown in Fig. 8(d) because a different habit plane is employed. The use of different habit planes is due to the consideration of different interfaces as shown in Fig. 7.

The instability of these three binary interfaces is a direct consequence of describing the system at $T = 0$ K where the bcc phase is energetically more favorable than the MIS or fcc, and bulk fcc phase is thermodynamically unstable against the MIS. Thus, to reduce the thermodynamic driving forces for the instability, the interface energy would have to be computed at temperatures close to the fcc → bcc transition temperature where the bulk energies become similar. This turns out to be unfeasible for such a complex system with the presently available *ab initio* approaches (see Section 5.4). Therefore, we try to avoid the unphysical relaxations due to the lattice instability by introducing constraints that fix the geometry of the corresponding bulk phases. Due to these constraints and the lack of temperature effects the resulting interface energy should be regarded as a way to identify trends only. A few of the thus constructed interface structures are shown in Fig. 9. When constructing these interfaces, the (100) plane shown in Fig. 1 is used as the habit plane.

Next to the lattice instability another issue we encounter is an electronic instability in the magnetic configuration. Trying to set up PM or antiferromagnetic (AFM) configurations for austenite or the MIS within the interface structure we systematically observe a breakdown of the electronic convergence. We therefore assume a FM state for the entire supercell to ensure a convergence of the electronic self-consistent calculations (see Section 5.3 for reasons why a FM state is chosen). The lattice constants at the interfaces are fixed to the bulk lattice constants of ferrite or cementite, respectively.

The energy gain of the interface by introducing the MIS in between is quantified as $[E_{\text{tot}}(\text{bcc(or cementite)} + \text{fct}) - E_{\text{tot}}(\text{bcc(or cementite)} + \text{MIS} + \text{fct}) - N(E(\text{fct}) - E(\text{MIS}))]/2A$, where N is the number of atoms of the MIS in the supercells (here $N = 2 \times 12 = 24$), and A is the interface area. E_{tot} is defined as the total energy of the entire supercell while E(fct) and E(MIS) refer to the bulk energy per atom. Consequently, we obtain the energy gain of the austenite/ferrite, and austenite/cementite interfaces by including the MIS as ∼139 and ∼129 meV/Å^2, respectively. The energies of the austenite/ferrite, and austenite/cementite interfaces in the absence of the MIS as a buffer layer are ∼336 and ∼283 meV/Å^2, respectively, i.e., approximately a factor of 2 higher. Thus, the above (approximate) model clearly shows that introducing the MIS as a buffer layer between either two bulk phases largely reduces the interface energy. Since atomic relaxation has to be excluded the interface energies computed here may be regarded as an upper limit to the real ones. As an intermediate structure between fcc and bcc Fe, the MIS contains both fcc- and bcc-like local coordinations. Hence, it can nicely link the different atomic orderings of austenite and ferrite at the interface. Moreover, the lattice parameters of the MIS have also certain flexibility and can vary between those of austenite and ferrite. Therefore, the MIS can also reduce the elastic strain energy due to the lattice mismatches to some extent.

In addition, to check if the interface can really stabilize the MIS, we also perform selective dynamics for the supercell shown in Fig. 9(a1) by allowing only 6 atomic layers (3 layers on each side) at the austenite/ferrite interface to relax and keeping the rest fixed. To ensure reliable electronic convergence, the magnetic state of the entire cell is still treated as FM. With this we clearly observe the MIS is formed at the austenite/ferrite interface, though it only

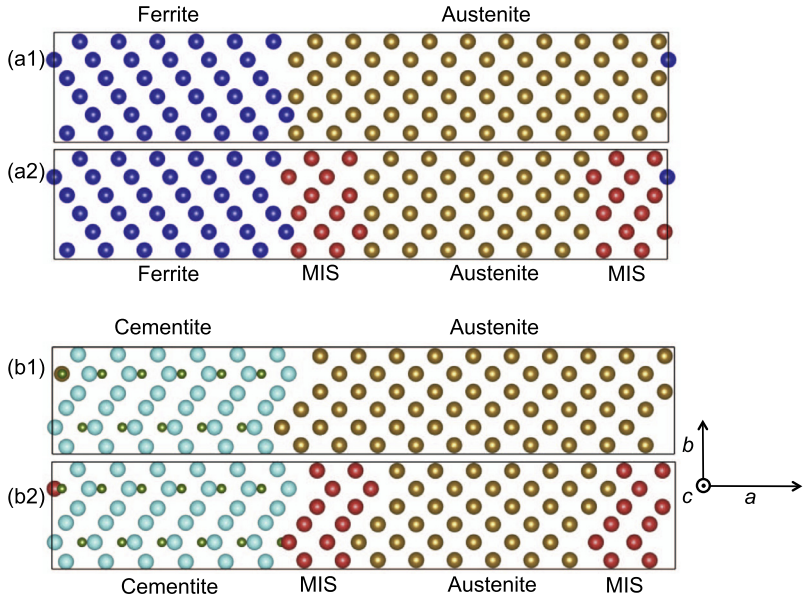

Fig. 9. Atomic structures of the interfaces. (a1) and (a2) show the interface between austenite and ferrite without and with the MIS, respectively. (b1) and (b2) show the interface between austenite and cementite without and with the MIS, respectively. The directions a, b and c are defined the same as those in Fig. 7.

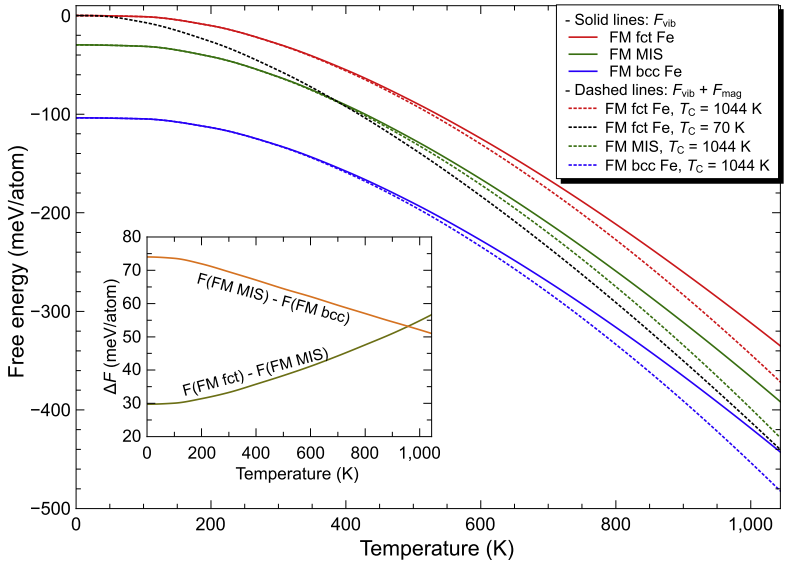

Fig. 10. Effect of temperature on the free energies of FM fct Fe, the MIS and bcc Fe including vibrational and magnetic entropy contributions. The vibrational entropy is evaluated by the quasi-harmonic Debye model and the magnetic entropy is estimated with the mean-field theory. For the inset plot, the energy difference includes both vibrational and magnetic contributions to the free energy. (For interpretation of the references to color in this figure caption, the reader is referred to the web version of this article.)

survives within 2–3 atomic layers. This means that the MIS does form within a finite thickness. It is not a stable bulk phase, but can be stabilized by the interface.

5.3. Magnetic state at the austenite/ferrite interface

The magnetic state at the interface between PM austenite and FM ferrite is rather complicated and there is no well defined experimental or theoretical evidence for a particular state. Hence, in our SSNEB simulations, we treat both austenite and the MIS as FM, and a PM relaxation is performed for comparison, with which we conclude that the formation of MIS is triggered by a FM ordering of austenite at the interface. This assumption has not only be introduced due to technical reasons, but is also physically justified if one considers the following arguments.

First, since the exchange parameter J of FM bcc Fe (~0.2 eV) is much larger than that of PM fcc Fe (close to 0) [46], the Fe atoms at the interface between PM austenite and FM ferrite are more strongly coupled to the FM ferrite side, and thus more likely to follow the FM ordering, known as the magnetic proximity effect [47–49]. This is also supported by a recent work from Razumov et al. [50], which reported that the short-range FM ordering in PM austenite is essential for the martensitic transformation of the Fe lattice.

Second, as reported by Okatov et al. [46], the exchange parameter J of fcc Fe shows a clear FM ordering with increasing volume and tetragonality. Therefore, the volume expansion and tetragonal distortion of the austenitic lattice at the austenite/ferrite interface can stabilize the local FM ordering and lower the elastic strain energy by reducing the large mismatch. Employing mean-field theory, we also evaluate the critical temperature of bulk Fe with respect to the c/a ratio based on the exchange parameters reported by Okatov. It is very clear that if one takes into account a tetragonal deformation of austenite, the critical temperature increases dramatically (There is also a change from Néel temperature to Curie temperature in between), which indicates the possibility of a magnetic transition in austenite prior to the structural transition at low temperatures during slow cooling.

Third, it has been reported [51–54], that the presence of interstitials in fcc Fe can trigger local FM ordering as well. In the case of cementite formation which requires a local C accumulation of 25 at.%, this further supports the formation of a local FM ordering of austenite at the interface.

In addition, any energy loss related the transition of a PM state to a FM state needs to be compared to the interface energy gain by forming the MIS at the austenite/ferrite interface.

In spite of the above arguments, there is no direct evidence for the magnetic treatment in this work. Hence, the local FM ordering at the austenite/ferrite interface is an assumption, which might involve an uncertainty. However, it is also notable here that the initial interface between austenite and ferrite is energetically very unfavorable mostly due to the remarkable lattice mismatches and different atomic arrangements. The magnetic state definitely affects the interface energy, but much less pronounced than the two other factors. Hence, even if one is able to simulate the interface between PM austenite and FM (or even PM) ferrite with *ab initio* techniques, similar behavior is still expected.

5.4. Finite temperature effects

As mentioned in Section 5.2 the temperature induced lattice vibrations and magnetic excitations play an important role in the phase transformations in Fe–C alloys. Hence, to evaluate the relevance of the $T = 0$ K calculations, finite temperature effects need to be taken into consideration. We carefully check the effect of temperature on the stabilities of phases in our system. Unfortunately, due to the dynamical instabilities of both the FM-HS fct Fe and FM MIS, and the convergence problems in describing finite temperature magnetic excitations, the highly accurate approaches for vibrational and magnetic entropy contributions developed by others and ourselves [55] are not applicable here. Instead, we employ the quasi-harmonic Debye model [56] for the lattice vibrations and the mean-field theory [57] for the magnetic excitations, respectively.

Fig. 10 shows the free energies of FM fct Fe, MIS and bcc Fe obtained by employing the above approaches. Considering first only vibrational excitations (solid lines) we clearly see that the relative stabilities of the three phases/structures are only slightly influenced by temperature. Since estimating the magnetic contribution requires as input the Curie temperature, which is unknown e.g., for the MIS, we consider several physically motivated choices: If we assume that the ferromagnetism is induced at the interface to ferrite for both fct Fe and the MIS, the respective Curie temperatures should be determined by the one of FM bcc Fe, i.e., 1044 K. Using this value we can observe that the relative stabilities of the three phases/structures remain qualitatively the same. A shortcoming of this simple estimate is that the bcc → fcc transition (occurring *in bulk* at 1185 K) is missing. This can be recovered if we take into account that the fcc phase is PM with a Néel temperature of 70 K (see black line in Fig. 10). Nevertheless, one should distinguish this bulk behavior from the local situation at the interface.

6. Conclusions

Our investigations provide a unified theory of the structural transformations among austenite, ferrite and cementite. While the focus of the discussion in this paper is on the displacive rearrangement of the Fe lattice, it yields at the same time a possible mechanism for the diffusional redistribution of C interstitials. Our theory gives therefore access to the coupling of these two seemingly incompatible aspects, which has so far been a challenge for atomistic simulations. The identification of the MIS is a direct consequence of these considerations. It is not only the result of a special OR or transformation path, but serves as a natural link in the atomistic decomposition of austenite into ferrite and cementite. This is due to the fact that it simultaneously provides a lattice correspondence between austenite, ferrite and cementite. As indicated by the solid state nudged elastic band calculations, the minimum energy paths of the structural transformations between the MIS and the three phases are triggered by the local C concentration, temperature, strain and magnetic ordering. The presently available atomistic simulation techniques are not sufficient to completely resolve their combined effect during the transformation and further method development is required to get a fully consistent description. Nevertheless, the present work provides clear indications that the MIS serves as an interface reconstruction, similar to the concept of complexions [11]. Hence it only exists at interfaces, where it continuously forms from austenite and evolves to ferrite and cementite depending on the local conditions, and thus leads to a moving interface scenario. In this way we obtain a clear atomistic picture of the phase transformation mechanisms among austenite, ferrite and cementite, which significantly improves our understanding how the initial stage of the decomposition process occurs. These mechanisms are assumed to trigger also the formation of complex microstructures in steels, such as pearlite and bainite.

Acknowledgements

We gratefully acknowledge financial supports of the Max-Planck Society within the SurMat Research School at the Max-Planck-Institut für Eisenforschung and of the Deutsche Forschungsgemeinschaft within the collaborative research centre SFB761 "Stahl – *ab initio*". We thank F. Körmann and B. Dutta for fruitful discussions and kind assistance.

References

[1] T. Yang et al., The structural transitions of Ti_3AlC_2 induced by ion irradiation, Acta Mater. 65 (2014) 351.
[2] M.J. Duarte, A. Kostka, J.A. Jimenez, P. Choi, J. Klemm, D. Crespo, D. Raabe, F.U. Renner, Crystallization, phase evolution and corrosion of Fe-based metallic glasses: an atomic-scale structural and chemical characterization study, Acta Mater. 71 (2014) 20.
[3] T. Frolov, S.V. Divinski, M. Asta, Y. Mishin, Effect of interface phase transformations on diffusion and segregation in high-angle grain boundaries, Phys. Rev. Lett. 110 (2013) 255502.
[4] M. Medarde et al., 1D to 2D Na^+ ion diffusion inherently linked to structural transitions in $Na_{0.7}CoO_2$, Phys. Rev. Lett. 110 (2013) 266401.
[5] C. Jiang, S.G. Srinivasan, Unexpected strain-stiffening in crystalline solids, Nature 496 (2013) 339.
[6] S. Moll, T. Jourdan, H. Lefaix-Jeuland, Direct observation of interstitial dislocation loop coarsening in α-Iron, Phys. Rev. Lett. 111 (2013) 015503.
[7] S. Griesser, M. Reid, Christian Bernhard, R. Dippenaar, Diffusional constrained crystal nucleation during peritectic phase transitions, Acta Mater. 67 (2014) 335.
[8] A. Dick, F. Körmann, T. Hickel, J. Neugebauer, Ab initio based determination of thermodynamic properties of cementite including vibronic, magnetic, and electronic excitations, Phys. Rev. B 84 (2011) 125101.

[9] L. Sandoval, H.M. Urbassek, P. Entel, The Bain versus Nishiyama–Wassermann path in the martensitic transformation of Fe, New J. Phys. 11 (2009) 103027.
[10] A.G. Khachaturyan, S.M. Shapiro, S. Semenovskaya, Adaptive phase formation in martensitic transformation, Phys. Rev. B 43 (1991) 10832.
[11] S.J. Dillon, M. Tang, W.C. Carter, M.P. Harmer, Complexion: a new concept for kinetic engineering in materials science, Acta Mater. 55 (2007) 6208.
[12] P.E. Blöchl, Projector augmented-wave method, Phys. Rev. B 50 (1994) 17953.
[13] J.P. Perdew, K. Burke, M. Ernzerhof, Generalized gradient approximation made simple, Phys. Rev. Lett. 77 (1996) 3865.
[14] G. Kresse, J. Furthmüller, Efficient iterative schemes for ab initio total-energy calculations using a plane-wave basis set, Phys. Rev. B 54 (1996) 11169.
[15] H.J. Monkhorst, J.D. Pack, Special points for Brillouin-zone integrations, Phys. Rev. B 13 (1976) 5188.
[16] M. Methfessel, A.T. Paxton, High-precision sampling for Brillouin-zone integration in metals, Phys. Rev. B 40 (1989) 3616.
[17] C.S. Roberts, Effect of carbon on the volume fractions and lattice parameters of retained austenite and martensite, Trans. AIME 197 (1953) 203.
[18] A. Udyansky, J. von Pezold, A. Dick, J. Neugebauer, Orientational ordering of interstitial atoms and martensite formation in dilute Fe-based solid solutions, Phys. Rev. B 83 (2011) 184112.
[19] E. Duman, M. Acet, E.F. Wassermann, J.P. Itié, F. Baudelet, O. Mathon, S. Pascarelli, Magnetic instabilities in Fe_3C cementite particles observed with Fe K-Edge X-ray circular dichroism under pressure, Phys. Rev. Lett. 94 (2005) 075502.
[20] A. van de Walle, G. Ceder, The alloy theoretic automated toolkit: a user guide, J. Phase Equilib. 23 (2002) 348.
[21] E.C. Bain, The nature of martensite, Trans. AIME 70 (1924) 25.
[22] G. Kurdjumov, G. Sachs, About the mechanism of hardening steel, Z. Phys. 64 (1930) 325.
[23] Z. Nishiyama, Mechanism of transformation from face-centred to body-centred cubic lattice, Sci. Rep. Res. Inst. Tohoku Univ. 23 (1934) 638.
[24] G. Wassermann, Einflu der α-γ-umwandlung eines irreversiblen nickelstahls auf kristall-orientierung und zugfestigkeit, Arch. Eisenhüttenwes. 6 (1933) 347.
[25] W. Pitsch, The martensite transformation in thin foils of iron–nitrogen alloys, Philos. Mag. 4 (1959) 577.
[26] A.B. Greninger, A.R. Troiano, Crystallography of austenite decomposition, Trans. AIME 140 (1940) 307.
[27] Y.A. Bagaryatsky, Veroyatnue mechanezm raspada martenseeta, Dokl. Akad. Nauk. SSSR 73 (1950) 1161.
[28] I.V. Isaichev, Orientatsiya tsementita v otpushchennoi uglerodistoi stali, Zh. Tekh. Fiz. 17 (1947) 835.
[29] N.J. Petch, The orientation relationships between cementite and α-iron, Acta Cryst. 6 (1953) 96.
[30] W. Pitsch, Der Orientierungszusammenhang zwischen Zementit und Ferrit im Perlit, Acta Cryst. 10 (1962) 79.
[31] W. Pitsch, Der Orientierungszusammenhang zwischen Zementit und Austenit, Acta Metall. 10 (1962) 897.
[32] S.W. Thompson, P.R. Howell, A preliminary comparison of two apparently diverse cementite/austenite orientation relationships, Scr. Metall. 21 (1987) 1353.
[33] M. Farooque, D. V. Edmonds, in: Proceedings of the XIIth International Congress for Electron Microscopy, San Francisco, 1990, p. 910.
[34] D.S. Zhou, G.J. Shiflet, A new orientation relationship between austenite and cementite in an Fe–C–Mn steel, Scr. Metall. 27 (1992) 1215.
[35] K.W. Andrews, The structure of cementite and its relation to ferrite, Acta Metall. 11 (1963) 939.
[36] K. Momma, F. Izumi, VESTA 3 for three-dimensional visualization of crystal, volumetric and morphology data, J. Appl. Crystallogr. 44 (2011) 1272.
[37] D. Sheppard, P. Xiao, W. Chemelewski, D.D. Johnson, G. Henkelman, A generalized solid-state nudged elastic band method, J. Chem. Phys. 136 (2012) 074103.
[38] G. Henkelman, H. Jónsson, Improved tangent estimate in the nudged elastic band method for finding minimum energy paths and saddle points, J. Chem. Phys. 113 (2000) 9978.
[39] D. Sheppard, R. Terrell, G. Henkelman, Optimization methods for finding minimum energy paths, J. Chem. Phys. 128 (2008) 134106.
[40] G. Krauss, Principles of the Heat Treatment of Steel, American Society for Metals, 1982.
[41] F. Körmann, A. Dick, T. Hickel, J. Neugebauer, Pressure dependence of the Curie temperature in bcc iron studied by ab initio simulations, Phys. Rev. B 79 (2009) 184406.
[42] C.S. Becquart, J.M. Raulot, G. Bencteux, C. Domain, M. Perez, S. Garruchet, H. Nguyen, Atomistic modeling of an Fe system with a small concentration of C, Comput. Mater. Sci. 40 (2007) 119.
[43] M. Rajagopalan, M.A. Tschopp, K.N. Solanki, Grain boundary segregation of interstitial and substitutional impurity atoms in alpha-iron, JOM 66 (2013) 129.
[44] S. Kauffmann-Weiss, M.E. Gruner, A. Backen, L. Schultz, P. Entel, S. Fähler, Magnetic nanostructures by adaptive twinning in strained epitaxial films, Phys. Rev. Lett. 107 (2011) 206105.
[45] Y.A. Du, L. Ismer, J. Rogal, T. Hickel, J. Neugebauer, R. Drautz, First-principles study on the interaction of H interstitials with grain boundaries in α- and γ-Fe, Phys. Rev. B 84 (2011) 144121.
[46] S.V. Okatov, Yu.N. Gornostyrev, A.I. Lichtenstein, M.I. Katsnelson, Magnetoelastic coupling in γ-iron investigated within an ab initio spin spiral approach, Phys. Rev. B 84 (2011) 214422.
[47] J. Hauser, Magnetic proximity effect, Phys. Rev. 187 (1969) 580.
[48] F. Maccherozzi et al., Evidence for a magnetic proximity effect up to room temperature at Fe/(Ga, Mn)As interfaces, Phys. Rev. Lett. 101 (2008) 267201.
[49] A.F. Kravets, A.N. Timoshevskii, B.Z. Yanchitsky, M.A. Bergmann, J. Buhler, S. Andersson, V. Korenivski, Temperature-controlled interlayer exchange coupling in strong/weak ferromagnetic multilayers: a thermomagnetic Curie switch, Phys. Rev. B 86 (2012) 214413.
[50] I.K. Razumov, D.V. Boukhvalov, M.V. Petrik, V.N. Urtsev, A.V. Shmakov, M.I. Katsnelson, Y.N. Gornostyrev, Role of magnetic degrees of freedom in a scenario of phase transformations in steel, Phys. Rev. B 90 (2014) 094101.
[51] N.I. Medvedeva, D. Van Aken, J.E. Medvedeva, Magnetism in bcc and fcc Fe with carbon and manganese, J. Phys.: Condens. Matter 22 (2010) 316002.
[52] D.W. Boukhvalov, Yu.N. Gornostyrev, M.I. Katsnelson, A.I. Lichtenstein, Magnetism and local distortions near carbon impurity in γ-Iron, Phys. Rev. Lett. 99 (2007) 247205.
[53] W. Pepperhoff, M. Acet, Constitution and Magnetism of Iron and Its Alloys, Springer, Berlin, 2001.
[54] D. Wu, H. Kahn, G.M. Michal, F. Ernst, A.H. Heuer, Ferromagnetism in interstitially hardened austenitic stainless steel induced by low-temperature gas-phase nitriding, Scr. Mater. 65 (2011) 1089.
[55] F. Körmann, B. Grabowski, B. Dutta, T. Hickel, L. Mauger, B. Fultz, J. Neugebauer, Temperature dependent magnon–phonon coupling in bcc Fe from theory and experiment, Phys. Rev. Lett. 113 (2014) 165503.
[56] M.A. Blanco, E. Francisco, V. Luaña, GIBBS: isothermal-isobaric thermodynamics of solids from energy curves using a quasi-harmonic Debye model, Comput. Phys. Commun. 158 (2004) 57.
[57] F. Körmann, A. Dick, B. Grabowski, B. Hallstedt, T. Hickel, J. Neugebauer, Free energy of bcc iron: integrated ab initio derivation of vibrational, electronic, and magnetic contributions, Phys. Rev. B 78 (2008) 033102.